Available online at www.sciencedirect.com
ScienceDirect
Proceedings of the Combustion Institute 31 (2007) 1711–1719
Proceedings of the Combustion Institute
www.elsevier.com/locate/proci

A consistent LES/filtered-density function formulation for the simulation of turbulent flames with detailed chemistry

Venkatramanan Raman [a,*], Heinz Pitsch [b]

[a] Department of Aerospace Engineering and Engineering Mechanics, The University of Texas at Austin, Austin, TX-78712, USA
[b] Center for Turbulence Research, Stanford University, CA 94305, USA

Abstract

A hybrid large-eddy simulation/filtered-density function (LES–FDF) methodology is formulated for simulating variable density turbulent reactive flows. An indirect feedback mechanism coupled with a consistency measure based on redundant density fields contained in the different solvers is used to construct a robust algorithm. Using this novel scheme, a partially premixed methane/air flame is simulated. To describe transport in composition space, a 16-species reduced chemistry mechanism is used along with the interaction-by-exchange with the mean (IEM) model. For the micro-mixing model, typically a constant ratio of scalar to mechanical time-scale is assumed. This parameter can have substantial variations and can strongly influence the combustion process. Here, a dynamic time-scale model is used to prescribe the mixing time-scale, which eliminates the time-scale ratio as a model constant. Two different flame configurations, namely, Sandia flames D and E are studied. Comparison of simulated radial profiles with experimental data show good agreement for both flames. The LES–FDF simulations accurately predict the increased extinction near the inlet and re-ignition further downstream. The conditional mean profiles show good agreement with experimental data for both flames.

Keywords: Large-Eddy simulation; Filtered-density function; Lagrangian approach; Detailed chemistry; Sandia flame series

1. Introduction

The increased demand for hydrocarbon-based energy coupled with environmental concerns have made simulation of turbulent combustion highly important. For simulation methods to be of practical value, it is essential to develop predictive tools that can provide quantitative solutions with minimal dependence on empirical constants used in the models. Large-Eddy simulation (LES) has dramatically increased the predictive capability of simulation schemes with regard to inert turbulent flows. LES resolves all large-scale features of the flow, and only models the small-scale motions that are deemed universal in inert flows. Chemical reactions typical of combustion occur at the smallest turbulent-scales thereby making this

* Corresponding author. Fax: +1 512 471 3788.
E-mail address: v.raman@mail.utexas.edu (V. Raman).

1540-7489/$ - see front matter © 2006 Published by Elsevier Inc. on behalf of The Combustion Institute.
doi:10.1016/j.proci.2006.07.152

universality assumption invalid. Hence, combustion and its interaction with the small-scales of turbulence have to be exclusively modeled. Several combustion models for LES have been proposed in the literature [1–4]. Recent reviews have been provided by Janicka and Sadiki [5] and Pitsch [6]. In the present work, a statistical approach based on the transported-probability density function model is used. It is well known that in such an approach, the chemical source terms appear closed and do not require modeling [7]. However, the sub-filter mixing needs to be modeled.

In the context of LES, the filtered-density function (FDF) is used as a statistical measure [8] instead of the probability density function (PDF). The joint-scalar FDF represents the instantaneous sub-filter scalar distribution in LES. Unlike a PDF which denotes a statistical property of the system in some averaged sense, the FDF is a fluctuating function that evolves with the flow [9–11]. A transport equation for the evolution of the FDF will span the physical as well as the compositional spaces and cannot be solved using conventional Eulerian discretization schemes [2,7]. Typically, a notional-particle based Lagrangian scheme is used where a large ensemble of particles are tracked in the computational domain. Since the joint-scalar FDF does not contain information regarding the turbulent velocity fields, a separate flow solver is required. For this reason, a hybrid technique [10,12] is followed in which the LES solver provides the turbulent flow field and the FDF scheme evolves the scalars. The Lagrangian scheme is computationally expensive since it requires that a stiff set of ordinary differential equations (ODE) be solved for each particle at each time-step to account for the combustion chemistry. Recent advances in numerical algorithms [13] combined with the availability of parallel computers have made this hybrid scheme a tractable [14] approach. However, practical use of the hybrid scheme is hindered by several numerical and modeling challenges. The main challenges of the FDF scheme are the consistent coupling of a statistical FDF solver with a deterministic LES solver and the lack of a universally valid sub-filter mixing model [11,14].

In this article, we describe a consistent formulation for the LES/FDF hybrid method. This formulation includes a dynamic formulation for the scalar time-scale appearing in the mixing model, which eliminates the used of modeling constants. This novel scheme is then used to simulate the Sandia D and E flame configurations. These flames are highly sensitive to the mixing model and the mixing-time-scale formulation [15,16]. Through detailed comparison with experimental data, the numerical accuracy and adaptability of this consistent scheme will be demonstrated.

2. LES/filtered-density function approach

The hybrid method consists of two separate solvers connected by a feedback mechanism. The LES scheme is time-accurate and hence requires that any solver that is coupled be time-accurate as well. In this section, we will describe the hybrid formulation and its numerical implementation, including the handling of the mixing model and the reaction source term.

2.1. Variable density low-Mach number LES solver

The filtering approach leads to the following modified Navier-Stokes equations that are solved in conservative form using the LES solver. In all known practical LES simulations, the filter is a box filter which implies that the filter is defined by the grid itself. The kernel definition satisfies the criterion that

$$\overline{\rho} = \int \rho\ G(\mathbf{y}-\mathbf{x})\,\mathrm{d}\mathbf{y}. \tag{1}$$

Applying this filter to the Navier-Stokes equation leads to the following filtered momentum equations

$$\frac{\partial \overline{\rho}}{\partial t} + \frac{\partial \overline{\rho}\widetilde{u}_\mathrm{j}}{\partial x_\mathrm{j}} = 0, \tag{2}$$

$$\frac{\partial \overline{\rho}\widetilde{u}_\mathrm{i}}{\partial t} + \frac{\partial \overline{\rho}\widetilde{u}_\mathrm{i}\widetilde{u}_\mathrm{j}}{\partial x_\mathrm{j}} = -\frac{\partial \tilde{P}}{\partial x_\mathrm{i}} + \frac{\partial \tau_\mathrm{ij}}{\partial x_\mathrm{j}} + \frac{\partial T_\mathrm{ij}}{\partial x_\mathrm{j}}, \tag{3}$$

where τ_ij is the viscous stress tensor given by

$$\tau_\mathrm{ij} = \widetilde{\mu}\left(\frac{\partial \widetilde{u}_\mathrm{i}}{\partial x_\mathrm{j}} + \frac{\partial \widetilde{u}_\mathrm{j}}{\partial x_\mathrm{i}} - \frac{2}{3}\frac{\partial \widetilde{u}_\mathrm{k}}{\partial x_\mathrm{k}}\delta_\mathrm{ij}\right) = 2\widetilde{\mu}\widetilde{S}_\mathrm{ij} \tag{4}$$

and $T_\mathrm{ij} = \overline{\rho}\widetilde{u}_\mathrm{i}\widetilde{u}_\mathrm{j} - \overline{\rho u_\mathrm{i} u_\mathrm{j}}$ denotes the sub-filter stresses.

The details of the solver are provided in [17]. The simulations presented below are performed in cylindrical coordinates with a semi-implicit formulation in the radial and azimuthal directions to avoid the time-step restrictions associated with such geometries [18]. Physical properties of the fluid namely, density and viscosity, are obtained from the FDF solver. The eddy viscosity is obtained from a dynamic Smagorinsky closure [19]. The LES solver also solves a scalar transport equation using a third-order upwind-biased scheme [20,17]. This additional scalar equation is used for the enthalpy feedback mechanism that will be described later. A dynamic procedure is used to obtain the sub-filter variance by employing the local equilibrium assumption [21].

The inlet boundary conditions for the LES solver are obtained from an independent pipe-flow simulations. The pipe-flow mass flow rate is matched to the experimental bulk flow rate. Using a periodic simulation, planes of velocity data at

successive time-steps are stored in a database and later incorporated in the LES simulation.

2.2. Lagrangian filtered-density approach

For variable-density flows, the filtered mass density function (FMDF) [2] can be defined as

$$F_{\mathrm{L}}(\boldsymbol{\psi};\mathbf{x},t)=\int_{-\infty}^{+\infty}\rho(\mathbf{y},t)\xi[\boldsymbol{\psi},\boldsymbol{\phi}(\mathbf{y},t)]G(\mathbf{y}-\mathbf{x})\,\mathrm{d}\mathbf{y}, \tag{5}$$

$$\xi[\boldsymbol{\psi},\boldsymbol{\phi}(\mathbf{y},t)]=\delta[\boldsymbol{\psi}-\boldsymbol{\phi}(\mathbf{y},t)], \tag{6}$$

where δ is an N-dimensional delta function for an N-species system and $\boldsymbol{\psi}$ is the random variable in the composition domain. For constant density flows, the FMDF will reduce to the FDF. In this work, we use the term FDF to describe both the FDF and the FMDF formulations. Equivalent to Eq. (1), the FMDF yields the following property:

$$\int_{-\infty}^{+\infty}F_{\mathrm{L}}\,\mathrm{d}\boldsymbol{\psi}=\int_{-\infty}^{+\infty}\rho(\mathbf{y},t)G(\mathbf{y}-\mathbf{x})\,\mathrm{d}\mathbf{y}=\overline{\rho}. \tag{7}$$

Similarly, the filtered mean of any scalar Q_ϕ can be defined as:

$$\widetilde{Q}_\phi=\int_{-\infty}^{+\infty}Q_\phi(\boldsymbol{\psi},\mathbf{y},t)F_{\mathrm{L}}\,\mathrm{d}\boldsymbol{\psi}. \tag{8}$$

Using these definitions, the transport equation for the joint composition FDF can be written as [2,22]

$$\begin{aligned}\frac{\partial F_{\mathrm{L}}}{\partial t}+\frac{\partial}{\partial\mathbf{x}}(\widetilde{\mathbf{u}}F_{\mathrm{L}})+\frac{\partial}{\partial\mathbf{x}}\left(\widetilde{\mathbf{u}'|\boldsymbol{\psi}}F_{\mathrm{L}}\right)\\ =-\frac{\partial}{\partial\boldsymbol{\psi}}\left[\left(\frac{1}{\overline{\rho}}\overline{\nabla\cdot\rho D\nabla\boldsymbol{\phi}|\boldsymbol{\psi}}+\mathbf{S}(\boldsymbol{\psi})\right)F_{\mathrm{L}}\right],\end{aligned} \tag{9}$$

where $\widetilde{\mathbf{u}}'|\boldsymbol{\psi}$ is the sub-filter velocity fluctuation conditioned on the scalar, $\overline{\nabla\cdot\rho D\nabla\boldsymbol{\phi}|\boldsymbol{\psi}}$ is the conditional micromixing term, and $\mathbf{S}$ is the reaction source term. The conditional velocity term is modeled using the gradient-diffusion hypothesis [2].

The FDF transport equation cannot be solved using conventional discretization schemes. Typically, a Lagrangian scheme is formulated where the computational domain is assumed to consist of uniformally distributed notional particles that evolve in physical and compositional spaces using stochastic differential equations. The evolution in physical space is through transport equations that use the filtered flow field from the LES solver:

$$\begin{aligned}d\mathbf{x}^*=&\left[\widetilde{\mathbf{u}}+\frac{1}{\overline{\rho}}\nabla\overline{\rho}(D+D_{\mathrm{T}})\right]\mathrm{d}t\\&+\sqrt{2(D+D_{\mathrm{T}})}\,\mathrm{d}\mathbf{W},\end{aligned} \tag{10}$$

where $\mathbf{x}^*$ is the instantaneous particle position. $\mathrm{d}\mathbf{W}$ is the Wiener diffusion term characterized by a Gaussian process with zero mean and variance of $\mathrm{d}t$, where $\mathrm{d}t$ is the time-step of the process. The velocity and turbulent diffusivity information are obtained from the LES solver, and interpolated onto the particle position. In this work, the simulations are performed in cylindrical coordinates requiring a transformation of the above equations.

The conditional mixing term requires modeling and has been the focus of research in FDF methods [11]. Based on theoretical considerations, a set of constraints can be specified for any mixing model to truly represent the micromixing terms [23]. However, none of the current models satisfies all the requirements [11,10]. Although several models have been used in practical simulations [24–27], the Interaction-by-Exchange-with-the-Mean (IEM) model is most commonly employed [25]. Here we use the IEM model. Then, transport in composition space is through mixing and reaction

$$\mathrm{d}\boldsymbol{\psi}=-\frac{1}{\tau_\phi}\left(\boldsymbol{\psi}-\widetilde{\boldsymbol{\phi}}\right)\mathrm{d}t+\mathbf{S}(\boldsymbol{\psi})\,\mathrm{d}t. \tag{11}$$

Here τ_ϕ is the scalar time-scale, which is usually evaluated from a turbulence time-scale τ from the assumption of a constant scalar-to-mechanical time-scale ratio C_ϕ as $\tau_p\,\mathrm{hi}=\tau/C_\phi$. A typical value for the time-scale ratio is $C_\phi=2$ [4]. In the past, it has been shown that simulation results are often sensitive to this model constant and different values have been used [15,28,16]. It is also clear that the time-scale ratio can be a function of space and time, and that it generally is a fluctuating quantity. Therefore, we will here use a dynamic model to directly evaluate τ_ϕ, thereby removing the need to specify the value of the mixing constant.

The model for the mixing time-scale is obtained from the dynamic models for the sub-filter variance and the scalar dissipation rate. The commonly used models for the conserved scalar variance and dissipation rate have the following form [21]:

$$\widetilde{Z''^2}=C_{\mathrm{Z}}\Delta^2\nabla\widetilde{Z}\cdot\nabla\widetilde{Z}, \tag{12}$$

$$\chi=2(\widetilde{D}+D_{\mathrm{T}})\nabla\widetilde{Z}\cdot\nabla\widetilde{Z}. \tag{13}$$

The sub-filter diffusivity D_{T} is determined using a dynamic procedure similar to that used to obtain the turbulent viscosity [19]. Using these relations, the scalar mixing time-scale can be computed as

$$\tau_\phi=\tau_{\mathrm{Z}}=\widetilde{Z''^2}/\chi=\frac{C_{\mathrm{Z}}\Delta^2}{2(\widetilde{D}+D_{\mathrm{T}})}, \tag{14}$$

where the mixing time-scale for all scalars is approximated by that of the mixture–fraction. Since D_{T} and C_{Z} are both obtained dynamically, this procedure removes the need to specify the constant C_ϕ. It is noted that using this formulation, the individual time-scales for the reactive scalars may also be computed. The scalar-dissipation rate model in Eq. (13) is based on the assumption that

production equals dissipation in the scalar variance equation. For reactive scalars, this relation could be modified to include the co-variance of scalar and scalar production rate appearing in the reactive scalar variance equation. This term is closed in the context of a transported FDF model. In the numerical implementation, the sub-filter variance is directly computed from the particle composition vector. Hence, the dynamic model for the variance is not required in the FDF context.

2.3. Coupling algorithm

In the low-Mach number approximation, acoustic pressure variations and the associated changes in density are neglected. The FDF solver evolves the thermochemical state of the local fluid and can thus provide the instantaneous density field. This is obtained from the particle thermochemical data ($\boldsymbol{\phi}_i$) and weight (w_i)

$$\overline{\rho}_p^{-1} = \sum_{i=1}^{N} w_i / \rho(\boldsymbol{\phi}_i), \tag{15}$$

where N denotes the particles in the control volume. Due to the stochastic nature of the FDF scheme, this density field will contain statistical noise. Hence, a direct feedback of the density field will lead to numerical instabilities. We solve this problem by using an Eulerian equivalent-enthalpy equation [29,14]. Here, an enthalpy equation is solved using an Eulerian scheme. The source term for this equation is provided using the FDF-based fields. By advancing the enthalpy equation in a time-consistent manner, the density change can be recovered from the equivalent-enthalpy. Such an indirect feedback is found to provide excellent numerical stability.

2.4. Numerical implementation

Each computational cell in the domain is seeded with a fixed number of particles, N_p. Each particle also carries a weight, w, that corresponds to the local fluid mass. Due to the varying grid volume, the particle number density will change with time and can adversely affect the statistical accuracy. To maintain this number

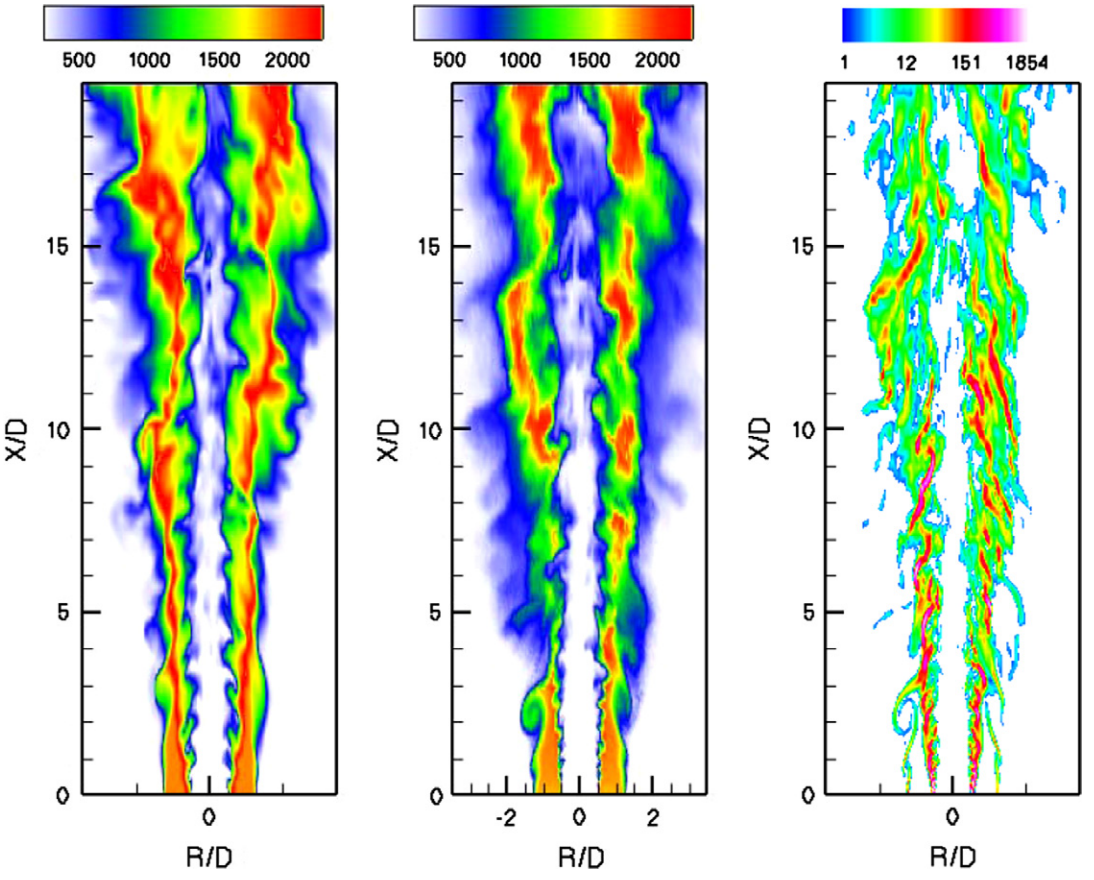

Fig. 1. Instantaneous temperature contours for flame D (left) and flame E (middle), and the scalar dissipation rate for flame E (right).

density within a specified range, splitting-clustering algorithms are employed [14]. Typical computational grids contain 1–2 million cells with N_p in the range of 30–50. To handle such large numbers of particles (50–500 million), parallel domain decomposition methods are employed. Further details of the implementation can be found in [14,16].

Integration of the chemical source term is a significant hurdle in LES/FDF simulations. Recent advances in computational methods have somewhat alleviated this problem [13,30]. In this work, we resort to direct integration using a stiff ODE solver, but employ certain simplification procedures. First, we limit direct integration only to particles with mixture–fraction in the range of 0.03–0.95. Composition vectors outside this range are advanced using a flamelet look-up table. It was found that using wider ranges did not affect the final results. In addition, we tabulate the direct integraton-based results in a single time-step and re-use the computations for all particles with compositions that are close to these tabulated points in composition space. This follows the ISAT scheme [13] in the basic formulation. However, we observe significantly less speedup in the range of 10–15 compared to typical ISAT speedups of 100–1000 [31]. Combined with the parallel implementation, this algorithm was sufficient to carry out the computations discussed here.

3. Simulation of Sandia flame series

The Sandia flame series [32] consists of a series of experiments using a piloted partially premixed flame configuration. The flames are studied using increasing inlet velocity of the fuel and oxidizer jets. The increased velocities increase the probability of local extinction. Here, we simulate the D and E flame configurations using a detailed description of the methane/air chemistry. Through the use of a dynamic model for the mixing time-scale, we remove the need to specify modeling constants *a priori* and compute the coefficients dynamically during the course of the simulation.

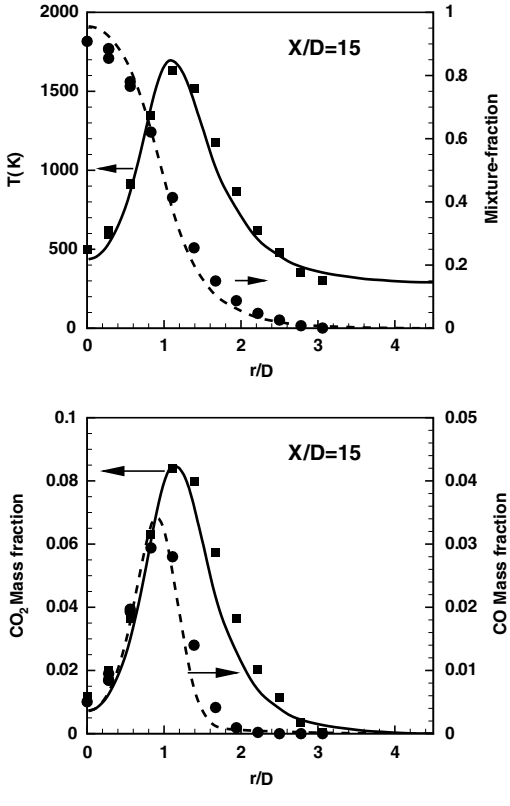

Fig. 2. Time-averaged radial profiles of species mass-fractions and temperature for flame D at $X/D = 15$. Symbols denote experimental data and lines denote simulation results.

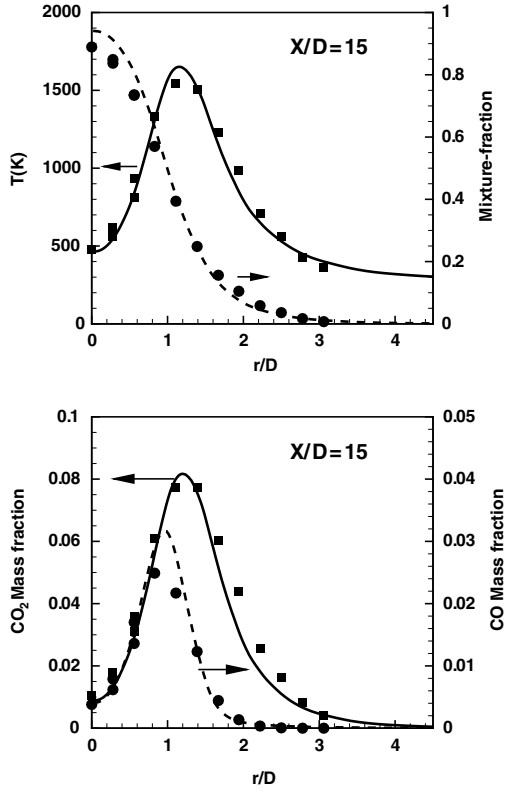

Fig. 3. Time-averaged radial profiles of species mass-fractions and temperature for flame E at $X/D = 15$. Symbols denote experimental data and lines denote simulation results.

The Sandia flame configuration consists of a central fuel jet with a diameter of 7.2 mm surrounded by a pilot flame with an outer diameter of 18.2 mm. A co-flow of air serves as the oxidizer. The fuel jet comprises of methane (25% by vol.) diluted in air (75% by vol.). The central jet velocity for flame D is 49.6 m/s while for flame E it is 74.4 m/s. The pilot issues at 11.4 m/s for flame D and 17.1 m/s for flame E. The co-flow velocity is fixed at 0.9 m/s for all cases. The simulations performed here use a 16-species chemistry mechanism reduced from the GRI-2.11 mechanism [33]. A $256 \times 128 \times 32$ computational grid was used in the simulations. The computational domain extended 80 jet diameters in the axial direction and 20 diameters in the radial direction. Grid clustering was used to refine the strong gradients near the inner shear layer formed between the fuel jet and the pilot as well as the outer shear layer formed between the pilot and the co-flow. The coupled simulations were performed with 40 particles per computational cell. Direct numerical integration of the chemical source term was used. The simulations were started from a statistically stationary flamelet-based solution. The FDF calculations with the chemical source term was continued for three residence times, where a residence time is defined as the time taken by a particle to move along the centerline from the inlet to the exit. Time-averaging was started after two residence time had passed.

Figure 1 shows instantaneous temperature distributions for flames D and E, as well as the instantaneous scalar dissipation rate for flame E. The temperature contours indicate that flame D has low levels of extinction while local extinction events are more common in flame E. Both these flames have relatively simple flow features with the reaction rate interlinked to the local strain in the two shear layers. Near the inlet, the presence of the pilot flame leads to enhanced stability with minimal extinction for both the flames. Further downstream, the outer co-flow and the inner fuel jet interact in the high-temperature region present in the shear layer. This configuration resembles a simple diffusion flame and has been widely studied using flamelet models [1,34]. It has been observed that although the laminar flamelet model does not predict the minor species accurately, the use of an unsteady flamelet model that takes into account

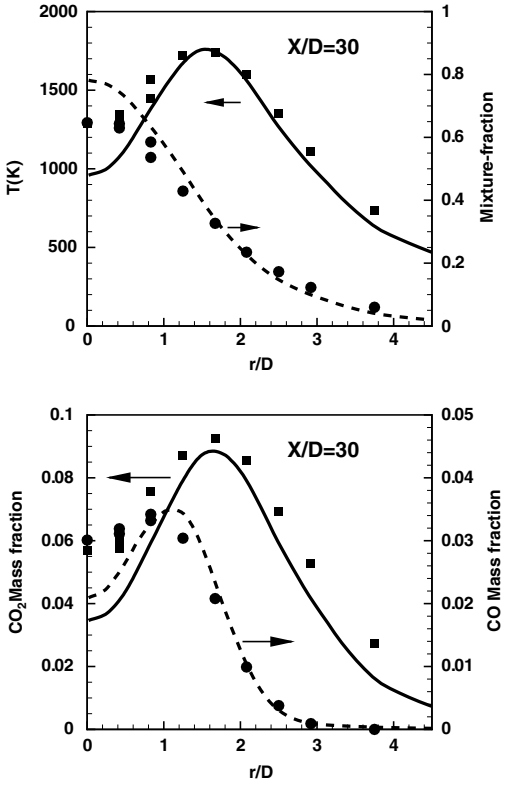

Fig. 4. Time-averaged radial profiles of species mass-fractions and temperature for flame E at $X/D = 30$. Symbols denote experimental data and lines denote simulation results.

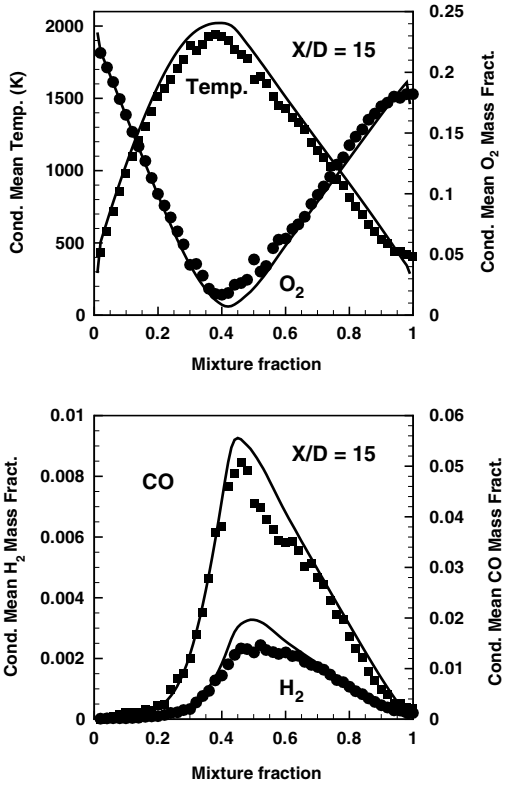

Fig. 5. Conditional mean temperature and species mass fraction for flame D.

the time-history of scalar dissipation rate fluctuations will enhance the predictive capability of the method [34].

The local regions of extinction in flame E extend over several grid-cells and exhibit length-scales comparable to the large-scales of the flow. The primary inception of the extinction region may be influenced by the mixing model used through quenching at the sub-filter level. However, it appears that these large pockets of extinction are linked to the local dissipation rate which exhibits coherent structures in the flow. In this regard, the mixing model may determine the cut-off dissipation rate at which sub-filter quenching is initiated. The instantaneous scalar dissipation rate contour also shows another interesting feature. Near the inlet, the large velocity differences between the streams creates a high strain-rate zone. However, the near-zero scalar gradients in the region of the pilot flame strongly reduce the scalar dissipation rate and prevent local extinction. Further downstream, persistent high scalar dissipation rates lead to local extinction with a high degree of correlation between the scalar dissipation rate and the locations of the extinction pockets.

Figures 2 and 3 show radial profiles of mixture–fraction, temperature and representative species for the two flame configurations at an axial location of $x/d = 15$. The simulation results are found to be in very good agreement with experimental data. Similar agreement is found at axial positions closer to the inlet. The figures indicate that both flames exhibit very similar unconditional mean profiles in spite of the increased levels of extinction observed in flame E. The profile of the mixture–fraction near the centerline indicates significant breakup of the core of the fuel jet. In both simulations, the predicted centerline mixture–fraction value is slightly higher than the experimental data. Figure 4 shows the mixture–fraction, temperature and species plots for flame E at $x/d = 30$. The mixture–fraction plot shows that the centerline decay of the fuel jet is underpredicted. Since the mixture–fraction values are still on the rich side, this leads to an underprediction of the centerline temperature as well as other species profiles. The reduced jet-spread leads to a faster radial decay of the mixture–fraction. This behavior is observed at other downstream positions as well.

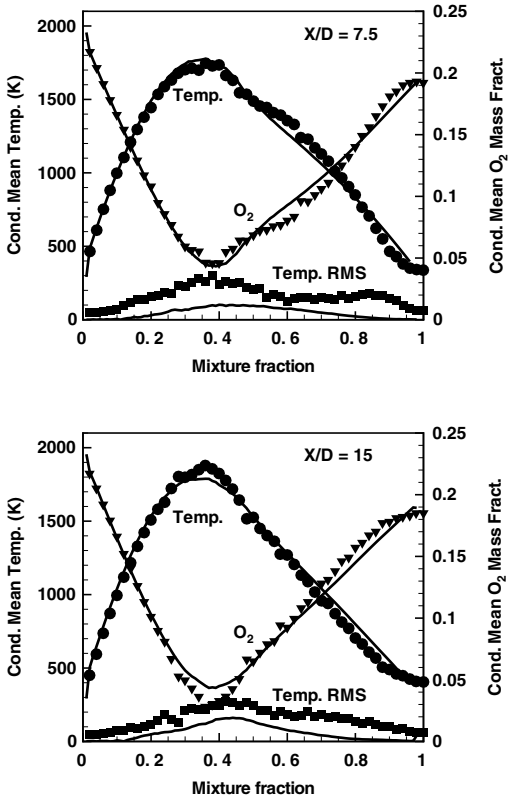

Fig. 6. Conditional mean temperature and O_2 mass fraction at two different axial locations for flame E.

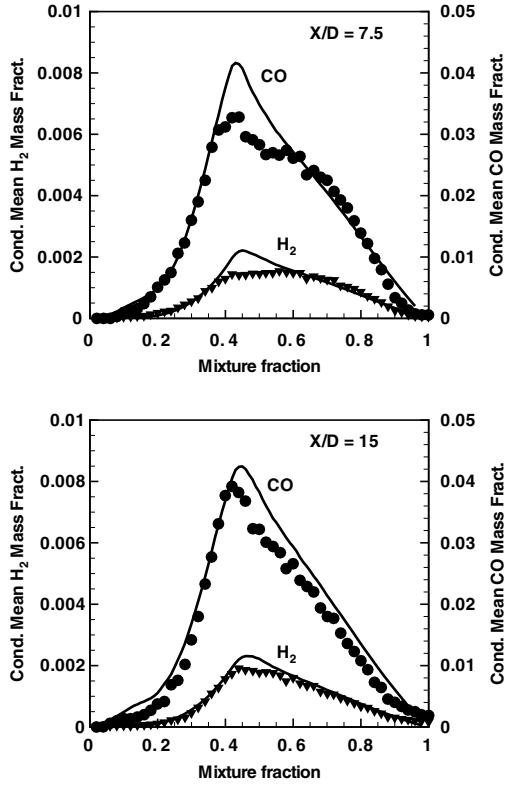

Fig. 7. Conditional mean CO and H_2 mass fraction at two different axial locations for flame E.

Figure 5 shows the conditional mean profiles for flame D. The results at this axial location are found to be representative of the other data stations as well. The conditional temperature plot shows that the peak temperature is slightly overpredicted which is consistent with the underprediction of the conditional O_2 mass fraction. The CO conditional mean shows good agreement with experimental data on the lean side, but shows some deviation from the experiments on the rich side. The trends are similar to those found in [34], where the time-history of scalar-dissipation rate fluctuations is considered. The conditional H_2 mean profile from the simulation shows an overprediction near $Z = 0.5$, but agrees well the experimental data at all other mixture–fraction values.

Figure 6 shows the conditional mean and RMS (root mean square) of temperature, and O_2 profiles for flame E at two different axial locations. At $x/d = 15$, there is significant amount of extinction observed both in the experiments and the simulations. This leads to the low consumption of O_2 and a reduction in the peak temperature compared to flame D (Fig. 5). The level of extinction is very well predicted by the simulation. A slight overprediction of extinction is observed near the stoichiometric mixture–fraction ($Z = 0.35$). The IEM mixing model is known to increase the extinction probability [15] and could lead to significant reduction in the re-ignition events. This would indicate that a similar overprediction of extinction should be present in flame D as well. Instead, the O_2 profile (Fig. 5) shows underprediction near the stoichiometric mixture fraction. This contradictory behavior seems to indicate that the time-scale model may be responsible for these small deviations. The conditional RMS of temperature is underpredicted at both the locations. This underprediction arises in part due to the local equilibrium assumption in the dynamic time-scale model. Additional error arises from the finite-volume representation of the production term. It is expected that a transport equation for the second-moment of the mixture–fraction combined with a dynamic localization model will provide a better representation of the unresolved energy. The conditional CO and H_2 mass fractions for flame E are shown in Fig. 7. Direct comparison with flame D profiles at $X/D = 15$ indicate that the peak in the CO profile is suppressed. At $X/D = 30$, strong re-ignition increases the peak CO profile. The predicted conditional H_2 mass fraction are in good agreement with experimental data at both locations. From the conditional data, it can be concluded that the simulations are able to capture the strong local extinction and the eventual re-ignition.

4. Conclusion

A consistent and robust LES–FDF algorithm has been proposed for the simulation of turbulent combustion. A 16-species reduced chemistry model is used with a modified direct integration procedure to reduce the computational expense. This is the first LES–FDF study that uses a realistic chemistry scheme to compute an experimental flame. Using this novel formulation, a partially-premixed flame experiment is simulated. A dynamic time-scale model was used along with the IEM mixing model to simulate two different flame configurations. This capability to simulate two different flame configurations without tuning model constants demonstrates the adaptability of this novel LES–FDF scheme. The results illustrate the numerical accuracy of the LES–FDF solvers, and show that this hybrid methodology is able to capture the different levels of extinction in the two configurations. Both conditional mean profiles and radial profiles showed good agreement with experimental data. By using a realistic chemistry mechanism it has been demonstrated that LES–FDF simulations of complex flames are feasible.

Acknowledgments

This research was carried out while V.R. was a Research Associate at the Center for Turbulence Research. The authors thank Prof. Rodney Fox for extensive discussions. Computer support from the NAS Supercomputing Center for performing the simulations is gratefully acknowledged.

References

[1] H. Pitsch, H. Steiner, *Phys. Fluids* 12 (10) (2000) 2541–2554.
[2] P.J. Colucci, F.A. Jaberi, P. Givi, *Phys. Fluids* 10 (2) (1998) 499–515.
[3] W.K. Bushe, H. Steiner, *Phys. Fluids* 11 (1999) 1896–1906.
[4] N. Peters, *Turbulent Combustion*, Cambridge University Press, 2000.
[5] J. Janicka, A. Sadiki, *Proc. Combust. Inst.* 30 (2005) 537–547.
[6] H. Pitsch, *Annu. Rev. Fluid. Mech.* 38 (2006) 453–482.
[7] S.B. Pope, *Combust. Sci. Tech.* 25 (1981) 159–174.
[8] S.B. Pope, *Computations of turbulent combustion: progress and challenges, in: Proceedings of the 23rd Symposium (International) on Combustion*, The Combustion Institute, Pittsburgh, 1990, pp. 591–612.
[9] D. Wang, C. Tong, *Phys. Fluids* 14 (7) (2002) 2170–2185.
[10] S.B. Pope, *Turbulent Flows*, Cambridge University Press, Cambridge, 2000.

[11] R.O. Fox, *Computational Models for Turbulent Reacting Flows*, Cambridge University Press, Cambridge, 2003.
[12] S.M. Correa, S.B. Pope, *Comparison of a Monte Carlo eps finite-volume mean flow model with bluff-body raman data, in: Twenty-Fourth Symposium (International) on Combustion*, Combustion Institute, Pittsburgh, 1992, pp. 279–285.
[13] S.B. Pope, *Combust. Theory Model.* 1 (1997) 41.
[14] V. Raman, H. Pitsch, R.O. Fox, *Combust. Flame* 143 (1–2) (2005) 56–78.
[15] J. Xu, S.B. Pope, *Combust. Flame* 123 (2000) 281–307.
[16] V. Raman, R.O. Fox, A.D. Harvey, *Combust. Flame* 136 (2004) 327–350.
[17] C.D. Pierce, Progress-variable approach for large-Eddy simulation of turbulence combustion, Ph.D. thesis, Stanford University, 2001.
[18] K. Akselvoll, P. Moin, *J. Fluid Mech.* 315 (1996) 387–411.
[19] P. Moin, K. Squires, W. Cabot, S. Lee, *Phys. Fluids A* 3 (1991) 2746–2757.
[20] B.P. Leonard, *Comp. Meth. Appl. Mech.* 19 (1979) 59–98.
[21] C.D. Pierce, P. Moin, *Phys. Fluids* 10 (1998) 3041–3044.
[22] F.A. Jaberi, P.J. Colucci, S. James, P. Givi, S.B. Pope, *J. Fluid Mech.* 401 (1999) 85–121.
[23] K. Tsai, R.O. Fox, *Ind. Eng. Chem. Res.* 37 (6) (1998) 2131–2141.
[24] R.L. Curl, *AIChE J.* 9 (1963) 175–181.
[25] J. Villermaux, L. Falk, *Chem. Eng. Sci.* 49 (24B) (1994) 5127–5140.
[26] J. Janicka, W. Kolbe, W. Kollmann, *J. Non-Equilib. Thermo.* 4 (1970) 47–66.
[27] S. Subramaniam, S.B. Pope, *Combust. Flame* 117 (1999) 732.
[28] R.P. Lindstedt, S.A. Louloudi, E.M. Vaos, *Proc. Combust. Inst.* 28 (2000) 149–156.
[29] M. Muradoglu, P. Jenny, S.B. Pope, D.A. Caughey, *J. Comput. Phys.* 154 (1999) 342–371.
[30] L. Lu, Z. Ren, V. Raman, S.B. Pope, H. Pitsch, *Investigation of strategies for the parallel implementation of isat in les/fdf/isat computations, in: 4th Joint Meeting of the U.S. Sections of the Combustion Institute*, The Combustion Institute, Philadelphia, PA, 2004.
[31] L. Lu, Z. Ren, V. Raman, S.B. Pope, H. Pitsch, LES/eps/ISAT computations of turbulent flames, in: Proceedings of the Summer Program 2004, Center for Turbulence Research, 2004, pp. 283–294.
[32] R.S. Barlow, J.H. Frank, *Effects of turbulence on specific mass fractions in methane/air jet flames*, *Twenty-Seventh Symposium (International) on Combustion* 27 (1998) 1087–1095.
[33] P. Pepiot, H. Pitsch, A 16-species reduced chemistry mechanism for combustion of methane/hydrogen fuel, unpublished (November 2004).
[34] H. Pitsch, *Proc. Combust. Inst.* 29 (2003) 1971–1978.

Comments

Johannes Janicka, *TU Darmstadt*, *Germany*. Could you provide us with additional information on how you dealt with the density treatment?

Reply. The direct feedback of density will cause numerical instabilities. For this reason, an extra filtered-enthalpy equation is solved using finite-volume methods. The source term for this equation is computed from the particle field. Finally, the LES density advancement is calculated using the enthalpy change at each time-step. Details of this implementation are found in Raman et al. ([14] in paper).

•

Alexander Y. Klimenko, *The University of Queensland*, *Australia*. The IEM model used for mixing has only a single parameter specifying intensity of the mixing. As you rightfully mentioned in your presentation, good simulations require matching the conditional variance in addition to matching the overall mixing rate. Have you thought about using another mixing model that would allow for adjustments in the production and dissipation rates of conditional variances?

Reply. The time-averaged conditional variance is generated by two components in LES—the resolved field and the sub-filter field fluctuations. Although the mixing model impacts the evolution of both these fields, the exact nature of the mixing model that will guarantee better agreement is not clear. However, we find in our study that the mixing time scale and the mixing model are very important. Different models therefore have to be assessed.